

Stability and decay of Bloch oscillations in the presence of time-dependent nonlinearityChristopher Gaul,¹ Elena Díaz,^{1,2} Rodrigo P. A. Lima,^{1,3} Francisco Domínguez-Adame,¹ and Cord A. Müller⁴¹*GISC, Departamento de Física de Materiales, Universidad Complutense, E-28040 Madrid, Spain*²*Institute for Materials Science, Technische Universität Dresden, D-01062 Dresden, Germany*³*Instituto de Física, Universidade Federal de Alagoas, Maceió AL 57072-970, Brazil*⁴*Centre for Quantum Technologies, National University of Singapore, Singapore 117543, Singapore*

(Received 13 September 2011; published 23 November 2011)

We consider Bloch oscillations of Bose-Einstein condensates in the presence of a time-modulated s -wave scattering length. Generically, the interaction leads to dephasing and decay of the wave packet. Based on a cyclic-time argument, we find—in addition to the linear Bloch oscillation and a rigid soliton solution—an infinite family of modulations that lead to a periodic time evolution of the wave packet. In order to quantitatively describe the dynamics of Bloch oscillations in the presence of time-modulated interactions, we employ two complementary methods: collective coordinates and the linear stability analysis of an extended wave packet. We provide instructive examples and address the question of robustness against external perturbations.

DOI: [10.1103/PhysRevA.84.053627](https://doi.org/10.1103/PhysRevA.84.053627)

PACS number(s): 03.75.Lm, 37.10.Jk, 52.35.Mw

I. INTRODUCTION

Quantum dynamics of atomic Bose-Einstein condensates (BECs) in optical lattices formed by counterpropagating laser beams [1–3] bears much resemblance to electron dynamics in solid-state crystals. For this reason and due to the vanishingly small contribution of decoherence effects, BECs are an ideal test ground for quantum transport of matter waves in complex environments. Perhaps one of the best examples are Bloch oscillations (BOs), a phenomenon predicted by Zener [4] based on the band-structure framework established by Bloch [5]: quantum particles in periodic potentials subjected to a constant force do not accelerate uniformly in real space, but oscillate instead. Because of defects and decoherence, BOs cannot be observed in conventional solids. With the mastery of ultracold atomic gases, however, BOs have been observed as a periodic motion of ensembles of ultracold atoms [6,7] and BECs [1–3] in tilted optical lattices.

The basic phenomenon of BOs can be well understood within a semiclassical framework. Let us consider a wave packet with a narrow momentum distribution in a lattice. If the wave packet is accelerated by a constant force $-F$ (like gravity for massive particles or an electric field for charged particles), then its momentum $\hbar k = -Ft$ will increase linearly. In a periodic potential with spatial period d , the dispersion relation of free particles is replaced with a band-structure dispersion ϵ_{nk} with band index n and quasimomentum k . In the tight-binding description, which is appropriate for a very deep lattice, the lowest-band dispersion reads $\epsilon_k \propto [1 - \cos(kd)]$. Now, quasimomentum and velocity are no longer proportional. Instead, a wave packet that is uniformly accelerated across the Brillouin zone has the group velocity $v_g \propto \partial_k \epsilon(k) \propto \sin(kd) = -\sin(\omega_B t)$, oscillating with the Bloch frequency $\omega_B = Fd/\hbar$. Consequently, the wave packet oscillates back and forth in real space. Also, related coherent phenomena have been realized with ultracold atoms. For instance, when the external force is modulated harmonically in time, the interwell tunneling of a BEC can be suppressed [8], as predicted theoretically in Ref. [9]. In addition, the simultaneous action of both constant and time-harmonic forces may lead to giant matter-wave oscillations called super BOs due to the beating of the usual BOs and the drive [10].

Because BOs rely on the coherent reflection of waves, they are very sensitive to any kind of dephasing generated by interaction effects or lattice imperfections. Any deviation from perfect periodicity causes random scattering of different k components of the wave packet. Thus, its momentum distribution starts to broaden and the coherent oscillations in real space are destroyed. This is the situation in crystalline solids, where the lattice spacing d is given by atomic distances, which are so short that electrons suffer from scattering events long before their quasimomentum reaches the Brillouin-zone edge π/d . One way to overcome this problem is to artificially increase the lattice spacing and thus shorten the Bloch period, as achieved in semiconductor superlattices [11,12].

Experiments with ultracold dilute gases offer very clean experimental conditions and open new possibilities. Atomic length scales are replaced by optical length scales. Atom-atom interactions—the main source of dephasing—are dominated by s -wave scattering. Many alkali-metal species (e.g., ⁷Li [13], ¹³³Cs [14,15]) allow tuning of the s -wave scattering length by means of a Feshbach resonance [14,16–18]. The s -wave scattering length can be tuned over a wide range, including a smooth crossover to negative values (i.e., attractive interaction). By suppressing the interaction entirely, one can observe very long-living BOs (up to 10^4 cycles in Ref. [15]). There are always residual experimental uncertainties, like a fluctuating s -wave scattering length, whose effect should be considered. Moreover, the scattering length can be deliberately modulated in time, which opens a pathway to new effects and interesting spectroscopic applications. For example, a harmonic modulation in time can be used to probe the collective excitations of trapped BECs [19,20].

In this work we present a detailed study of the stability and decay of BOs in tilted optical lattices for BECs with an atom-atom contact interaction that is modulated harmonically in time. Throughout the article, we discuss all results in the BEC context. But we like to emphasize from the outset that our analysis is based on mathematical properties of the nonlinear Schrödinger equation and thus applies to all physical systems governed by equation (5) below. In particular, a very clean realization is provided by one-dimensional (1D) lattices of optical waveguides [21–23]. In previous work [24,25], we

identified an infinite family of harmonic modulations $g(t)$ that guarantee long-living BOs on the mean-field level. We studied both the stable and unstable cases by using, respectively, a collective-coordinates (CC) approach [26] as well as linear stability analysis within Floquet theory [27]. In this article, we rederive these results in greater detail and extend them in several important aspects.

The paper is organized as follows: In Sec. II we introduce the tight-binding approximation to the Gross-Pitaevskii description, suitable for BECs in deep optical lattices. A numerical solution of the discrete Gross-Pitaevskii equation with time-harmonic s -wave scattering length shows the occurrence of stable and unstable dynamics of the BEC, depending on the frequency and phase of the modulation. In Sec. III we prove, within the smooth-envelope approximation, the existence of an infinite family of interactions leading to stable BOs, which is at odds with the quasistatic soliton stability criterion. We generalize the cyclic-time argument developed in Ref. [25] to cover all the solutions found by a different method in Ref. [24] and derive the limit of validity of the wide-envelope ansatz. Next, Sec. IV recapitulates the CC approach of Ref. [24] and improves the physical interpretation in terms of the momentum variance. The impact of several relevant modulations of the interaction is discussed in detail. The CC approach captures satisfactorily the effects of time-dependent atom-atom interactions, as long as the wave-packet shape is essentially preserved. The decay of BOs under unstable modulations is described in Sec. V, where we develop a linear stability analysis of wide wave packets. Via perturbative Floquet theory, we study the growth of perturbations that ultimately destroy the wave packet. Here, we cover a wider class of unstable perturbations than presented in Ref. [25]. After discussing the respective regimes of validity of our approaches, we summarize and conclude the article in Sec. VI.

II. MEAN-FIELD TIGHT-BINDING MODEL

In typical BEC experiments, atomic gases are very dilute, in the sense that the interparticle spacing exceeds the s -wave scattering length, which allows for a description within Gross-Pitaevskii theory [28]. The condensate is initially created in a harmonic trap and then loaded into an optical lattice potential $V(\mathbf{r})$ with transverse confinement [15]. The condensate amplitude $\Psi(\mathbf{r}, t)$ then evolves according to the Gross-Pitaevskii equation

$$i\hbar \frac{\partial}{\partial t} \Psi(\mathbf{r}, t) = \left[-\frac{\hbar^2}{2m} \nabla^2 + V(\mathbf{r}) + Fz \right] \Psi(\mathbf{r}, t) + g_{3D} |\Psi(\mathbf{r}, t)|^2 \Psi(\mathbf{r}, t). \quad (1)$$

The homogeneous force F describes a uniform acceleration (e.g., by gravity) along an axis, which we take to be the z axis. Even in the absence of the force F , the initial wave packet is not the ground-state configuration, and the condensate tends to spread across the lattice. In the case of repulsive self-interaction $g_{3D} = 4\pi\hbar^2 a_s/m > 0$ (a_s is the s -wave scattering length), this tendency is enhanced. In the opposite case $a_s < 0$, self-attraction counteracts dispersion and allows for soliton solutions [13].

Since the phenomenon of BOs takes place only in the longitudinal z direction, we consider a lattice potential with strong transverse confinement, such that the transverse degrees of freedom remain frozen in their harmonic-oscillator ground state. In particular, we exclude from our study the regime of weak transverse confinement that results in stacks of pancake-shaped BECs. These are prone to transverse excitations in the presence of the time-dependent, sign-changing nonlinearity that we consider below. For an extensive study of the excitation of transverse degrees of freedom, see Ref. [29]. Integrating out the transverse degrees of freedom then results in the one-dimensional Gross-Pitaevskii equation

$$i\hbar \frac{\partial}{\partial t} \Psi_{1D}(z, t) = \left[-\frac{\hbar^2}{2m} \partial_z^2 + V_{1D}(z) + Fz \right] \Psi_{1D}(z, t) + g_{1D} |\Psi_{1D}(z, t)|^2 \Psi_{1D}(z, t), \quad (2)$$

with the effective interaction parameter $g_{1D} = m\omega_{\perp} g_{3D}/(2\pi\hbar)$ [30]. In order for Eq. (2) to be valid, the transverse oscillator energy $\hbar\omega_{\perp}$ must exceed all other relevant energies.

If the potential $V_{1D}(z) = V_0 \sin^2(\pi z/d)$, with lattice constant d , amplitude $V_0 > 0$, and local oscillator frequency $\omega_{\parallel} = \pi\sqrt{2V_0/m}/d$, is sufficiently deep, only the local harmonic oscillator ground state (or Wannier function of the lowest band) of each lattice well is populated. The condensate is represented by the complex amplitudes Ψ_n for occupying the lattice wells centered at $z_n = nd$. A tight-binding equation of motion is found by integrating also over the z coordinate:

$$i\hbar \dot{\Psi}_n = -J(\Psi_{n+1} + \Psi_{n-1}) + Fdn\Psi_n + g|\Psi_n|^2\Psi_n. \quad (3)$$

Neighboring sites are coupled by the tunneling matrix element $J \approx 4\pi^{-1/2} E_r (V_0/E_r)^{3/4} \exp(-2\sqrt{V_0/E_r})$, where $E_r = \hbar^2\pi^2/(2md^2)$ is the recoil energy [30]. The tight-binding interaction parameter $g = N\sqrt{m\omega_{\parallel}}/(2\pi\hbar)g_{1D}$ contains the total number of particles N because we choose to normalize the discrete wave function as $\sum_n |\Psi_n|^2 = 1$. Equation (3) is valid only for very deep transverse and longitudinal trapping potentials, for which $\hbar\omega_{\parallel}, \hbar\omega_{\perp} \gg \|\mu\|_{\infty}$, where $\|\mu\|_{\infty} = \max_n |g\Psi_n^2|$ is the maximum local mean-field interaction energy. Under these conditions the shape of the local wave functions does not depend much on the occupation [26,31], and the tight-binding parameters J and g are also not affected.

The tight-binding description (3) is equivalent to a single-band description and thus neglects Landau-Zener tunneling (LZT) to higher bands. Let us briefly discuss the conditions under which this approximation is valid. In the linear case ($g = 0$), LZT can be neglected if the band gap $E_{\text{gap}} = V_0/2$ [30,32] is large enough or, more precisely, if [33]

$$FdE_r \ll E_{\text{gap}}^2. \quad (4)$$

In the case of constant interaction, the effective lattice potential is rescaled by a factor $(1 + 4E_{\text{int}}/E_r)^{-1}$ [3], reducing the band gap by the same factor. A typical experimental value of $V_0 = 4E_r$ results in $E_r/J = 8.55 \gg E_{\text{int}}/J = g|\Psi_n|^2 \lesssim 0.1$ for typical parameters chosen below (see, e.g., Fig. 1). Thus, we find that the relative correction to the lattice potential E_{int}/E_r is smaller than 1.2%, which does not change the previous validity condition (4). Finally, in the case of a modulated interaction [e.g., $g(t) = g_0 \cos(\omega t + \phi)$], one first has to ensure that the interaction energy remains smaller than

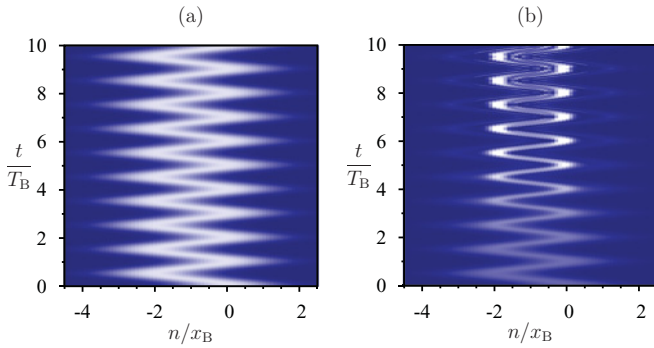


FIG. 1. (Color online) Condensate density $|\Psi_n(t)|^2$ as a function of position and time, obtained by numerical integration of Eq. (5). Initially, the wave packet is at rest and has the Gaussian shape (6) with width $\sigma_0 = 10$ chosen equal to the amplitude $x_B = 2/F$, $F = 0.2$, of free BOs. Two different harmonically modulated nonlinearities (a) $g(t) = g_0 \cos(Ft)$ and (b) $g(t) = g_0 \sin(Ft)$ with $g_0 = 1$ result in (a) stable and (b) unstable oscillations, respectively.

the gap. For the same parameters, this results in $E_{\text{int}}/J \ll E_{\text{gap}}/J = 17.1$, which is well fulfilled. Second, the modulation frequency should not become resonant with the gap. Below, we consider frequencies ω of the same order as the Bloch frequency Fd/\hbar . Thus, with V_0/E_r of order one, the condition $\hbar\omega \ll E_{\text{gap}}$ is already included in Eq. (4), which finally turns out to also be the relevant condition in the nonlinear cases. We conclude that LZT can be neglected in the situations considered for this work, and that the single-band description (3) is justified.

Hereafter we take the lattice constant d and tunneling J as the units of length and energy, respectively, and set $\hbar = 1$. Equation (3) then takes the form

$$i\dot{\Psi}_n = -\Psi_{n+1} - \Psi_{n-1} + Fn\Psi_n + g(t)|\Psi_n|^2\Psi_n. \quad (5)$$

In the noninteracting case $g = 0$, the atomic cloud oscillates with the Bloch frequency $\omega_B = 2\pi/T_B = F$ and amplitude $x_B \approx 2/F$ (in the chosen units), as we recall in Sec. III A below. A constant nonlinearity $g \neq 0$ is known to rapidly dephase Bloch oscillations [15,21,26,34]. Our notation $g(t)$ emphasizes that we are interested in the effects of an interaction that is modulated in time. In cold atomic gases, this can be realized by means of an external magnetic field close to an appropriate Feshbach resonance [14,16–18]. In arrays of nonlinear optical waveguides, which also allow for a tight-binding description like (5), time is equivalent to the propagation distance along the waveguides, and $g(t)$ could be realized as a spatially modulated cubic nonlinearity [21,35].

In order to provide a foretaste of the interesting effects that such a time-dependent interaction can have, we solve Eq. (5) numerically by means of the fourth-order Runge-Kutta method for a wave packet with an initial Gaussian shape:

$$\Psi_n(0) = (2\pi\sigma_0^2)^{-1/4} \exp(-n^2/4\sigma_0^2). \quad (6)$$

Figure 1 shows the condensate density $|\Psi_n(t)|^2$ as a function of position and time for two different harmonic interactions: [Fig. 1(a)] $g(t) = g_0 \cos(Ft)$ and [Fig. 1(b)] $g(t) = g_0 \sin(Ft)$. In the first case (a), the Gaussian shape is preserved over time, and the interacting condensate performs long-living BOs with frequency $\omega_B = F$. In the second case (b), the initial shape

is destroyed after a few cycles, as the wave function develops satellite peaks, and BOs are rapidly destroyed.

These two cases differ solely by the relative phase between the interaction modulation and the linear Bloch oscillation, which defines a reference time starting at $t = 0$ when the wave packet is at rest. Strikingly, in the stable case [Fig. 1(a)], the strongest repulsion $g = +g_0$ coincides with the upper turning point of the wave packet (i.e., when the momentum is at the center of the Brillouin zone and the positive mass disperses the wave packet). The strongest attraction $g = -g_0$ occurs at the lower turning point (i.e., with the momentum at the Brillouin zone edge and negative mass contracting the wave packet). Therefore, the observed stability clearly contradicts the simple quasistatic criterion, according to which stable BOs should occur when the nonlinearity compensates the lattice dispersion, instead of adding to it [36].

The results shown in Fig. 1 prompt at least the following questions, for which we will provide the answers: (i) Which are the periodic modulations $g(t)$ that lead to stable BOs? In the upcoming Sec. III, we use symmetry considerations to identify a family of stable modulations. (ii) How does the interaction affect the shape of an oscillating wave packet, both in the stable and unstable cases? Section IV describes a variational approach in terms of collective coordinates, which provides a first set of quantitative answers. (iii) How robust are the stable cases against small experimental imperfections? In Sec. V, we develop a linear stability analysis for periodic perturbations using Floquet theory, which provides a second, complementary set of answers that is in excellent agreement with the numerics.

III. CYCLIC-TIME SOLUTIONS FOR WIDE WAVE PACKETS

In all of the following, we consider wide wave packets, which span many lattice sites, as obtained by adiabatically loading an extended BEC from a shallow trap into an optical lattice [15]. The first effect of the mean-field tight-binding equation (5) is to imprint a phase factor $\exp(-iFnt)$ onto each amplitude Ψ_n . Such a phase factor can be separated from a smooth envelope $A(z, t)$ centered on the moving reference point $x(t)$ by the ansatz

$$\Psi_n(t) = e^{ip(t)n} A(n - x(t), t) e^{i\phi(t)}. \quad (7)$$

The equation of motion obeyed by the envelope $A(z, t)$ is found by Taylor-expanding the hopping terms of Eq. (5) as $\Psi_{n\pm 1} = e^{\pm ip} (A \pm \partial_z A + \partial_z^2 A/2) e^{ipn + i\phi(t)}$, with third and higher-order derivatives of A assumed to be negligible (Section III D below discusses the validity of this assumption). The force term is taken care of by choosing

$$p(t) = -Ft, \quad (8)$$

for the initial condition $p(0) = 0$. The first spatial derivative $\partial_z A$ can be eliminated by setting

$$x(t) = \frac{2}{F} [\cos(Ft) - 1], \quad (9)$$

such that $x(0) = 0$ and $\phi(t) = 2 \sin(Ft)/F$ with $\phi(0) = 0$ without loss of generality. These choices describe the uniform motion of the quasimomentum across the Brillouin zone and the resulting BO in real space. During this oscillation, the

envelope is found to obey the nonlinear Schrödinger equation (NLSE)

$$i\partial_t A = -\frac{1}{2m(t)}\partial_z^2 A + g(t)|A|^2 A, \quad (10)$$

with the oscillating inverse mass $m(t)^{-1} = 2\cos(Ft)$. Before analyzing the effect of a modulated interaction $g(t)$ in Sec. III B, we first describe the usual linear BOs in the absence of interaction ($g = 0$), while paying particular attention to the internal breathing dynamics.

A. Linear Bloch oscillation with breathing

In the linear case $g = 0$, Eq. (10) is the Schrödinger equation for a free particle with oscillating inverse mass $m(t)^{-1} = 2\cos(Ft)$. This problem can be mapped to the even-simpler case of constant mass by introducing the cyclic time

$$\eta(t) = \frac{\sin Ft}{F}. \quad (11)$$

Since $\partial_t \eta = \cos(Ft)$, the oscillating mass drops out of the resulting equation of motion $i\partial_\eta \tilde{A} = -\partial_z^2 \tilde{A}$ for $\tilde{A}(z, \eta(t)) = A(z, t)$. This is the simplest free-particle Schrödinger equation, whose solution reads $\tilde{A}_k(\eta) = \exp(-ik^2\eta)\tilde{A}_k(0)$ in the momentum representation. The real-space solution at cyclic time η is the initial wave packet $\tilde{A}(z, 0) = A(z, 0)$ propagated with the unitary evolution operator in the position representation, which is a Gaussian. Under this evolution, an initial Gaussian envelope $\tilde{A}(z, 0) = \Psi_z(0)$ such as (6) stays Gaussian:

$$\tilde{A}(z, \eta) = \frac{\sqrt{\sigma_0}}{\sqrt[4]{2\pi\tilde{\sigma}(\eta)}} \exp\left[-\frac{z^2}{4\tilde{\sigma}(\eta)^2}\right]. \quad (12)$$

The complex width $\tilde{\sigma}(\eta)^2 = \sigma_0^2 + i\eta$ is monotonic in the cyclic time η . But expressed in the physical time $\eta(t) = \sin(Ft)/F$, the evolution is necessarily periodic:

$$A(z, t) = \frac{\sqrt{\sigma_0}}{\sqrt[4]{2\pi\hat{\sigma}(t)}} \exp\left[-\frac{z^2}{4\hat{\sigma}(t)^2}\right], \quad (13)$$

where $\hat{\sigma}(t)^2 = \sigma_0^2 + i\sin(Ft)/F$. This solution describes a wave packet centered at $z = 0$ with variance

$$\sigma(t)^2 = \int dz z^2 |A(z, t)|^2 = \sigma_0^2 + \frac{\sin(Ft)^2}{F^2\sigma_0^2}. \quad (14)$$

The wave packet broadens only initially. At $Ft = \pi/2$ (i.e., after the first quarter of the Bloch cycle), the mass changes sign and the time evolution of the width is reversed. At the edge of the Brillouin zone $Ft = \pi$, the wave packet recovers its original shape. Thus, the wave packet shows perfectly periodic breathing on top of the BO; instead of dispersing, it remains localized due to the combination of lattice and tilt. The relative amplitude of the breathing (14) is $1/(F\sigma_0^2)^2$, which should be very small for the smooth-envelope equation (10) to be valid.

The above discussion of the linear BO is based on the NLSE (10), which neglects higher derivatives (i.e., assumes that the wave packet is smooth and wide). As we will discuss in Sec. III D, the linear BO remains periodic beyond that assumption, even for very narrow wave packets. With decreasing width, the breathing increases and the real-space Bloch amplitude is reduced until it approaches zero [37,38].

B. Bloch-periodic interaction

As shown already by the noninteracting solution (13), a Bloch-oscillating wave packet can display rich internal dynamics with initial broadening, provided that it recovers its initial state at the end of the Bloch period. To begin with, we recall the cyclic-time argument developed in Ref. [25] and identify those modulations $g(t)$ which are Bloch periodic and guarantee stable BOs. Later, in Sec. III C, we extend this reasoning to arbitrary (rational) frequency ratios.

1. General case

Motivated by the BO stability for $g(t) \propto \cos(Ft)$ observed in Fig. 1, we consider the class of Bloch-periodic interactions that are a product of $\cos(Ft)$ and any function $P(\eta)$ of the cyclic time $\eta = \sin(Ft)/F$ alone:

$$g(t) = \cos(Ft)P(\eta(t)). \quad (15)$$

Notably, this family includes the higher harmonics $g(t) = g_0 \cos[(2n+1)Ft]$ and $g(t) = g_0 \sin(2nFt)$ for all integer n (as well as all linear combinations thereof), because they can always be brought into the form (15) with the help of trigonometric identities. $\tilde{A}(z, \eta(t)) = A(z, t)$ then obeys the equation of motion

$$i\partial_\eta \tilde{A} = -\partial_z^2 \tilde{A} + P(\eta)|\tilde{A}|^2 \tilde{A}, \quad (16)$$

which depends only on the cyclic time η . And no matter the detailed form of its solution $\tilde{A}(z, \eta)$, since $\eta(t)$ is a *periodic function of time*, the solution $A(z, t)$ must be periodic as well. Just as in the linear case discussed in Sec. III A above, the envelope time evolution over the first quarter of every Bloch period will be exactly reversed during the second quarter.

The family of interactions (15) includes the cases $g(t) = \pm g_0 \cos(Ft)$, but not $\pm g_0 \sin(Ft)$, which is a first explanation of the strikingly different behavior exhibited in Figs. 1(a) and 1(b). In the latter case, the equation of motion cannot be written in terms of η alone, so that the cyclic-time argument does not apply. Of course, this fact by itself does not necessarily imply that modulation (b) is unstable, but Secs. IV and V below will show that this is indeed the case.

2. Special case: rigid soliton

Let us for a moment consider the NLSE (10) from a quasistatic point of view (i.e., take mass m and interaction g as constant). In the usual case of positive mass, a linear wave packet disperses. This dispersion has to be compensated by an attractive interaction in order to obtain a stationary wave packet. For a negative mass (e.g., quasimomentum close to the band edge), a repulsive interaction is needed in order to prevent the wave packet from contracting. If mass and interaction have opposite signs, the NLSE (10) admits a stable soliton solution [39]:

$$A(z, t) = \frac{1}{\sqrt{2\xi}} \frac{1}{\cosh(z/\xi)} e^{-i\omega t}, \quad (17)$$

with a characteristic width $\xi = -2/(gm) > 0$.

Such a soliton configuration can be maintained during the BO if the interaction g is modulated such that its sign is always opposite to the sign of the mass [40]. However,

the mere existence of a soliton configuration at all times is not sufficient for the preservation of the wave packet. If the equilibrium width $\xi(t) = -2/[m(t)g(t)]$ changes rapidly in time, the soliton cannot evolve adiabatically, and internal degrees of freedom are excited, which will finally destroy the soliton. Therefore, the simplest way to preserve a long-living wave packet is to have no internal dynamics at all. To this aim, the interaction parameter is modulated such that the equilibrium width ξ_0 is constant [i.e., $g_r(t) = -|g_r| \cos(Ft)$ where $|g_r| = 4/\xi_0$]. Hereafter, this case will be referred to as the *rigid soliton*.

In fact, our previous discussion shows that the rigid soliton is but a special member of the more general family of stable solutions. The stable interaction of Fig. 1(a), $g(t) = +|g_0| \cos(Ft)$, enhances the breathing of the linear BO, while the modulation $g(t) = -|g_0| \cos(Ft)$ tends to suppress it, even causing antibreathing for $|g_0| > |g_r|$. Clearly, the $-\cos$ case fulfills the soliton stability criterion $m(t)g(t) < 0$ for all times, whereas the $+\cos$ case does not. The preceding time-reversal argument, however, assures that both of them lead to undamped BOs—at least within the approximations underlying the NLSE (10). Thus, while the rigid-soliton criterion is sufficient for stability, it is by no means necessary.

C. Bloch-commensurate interaction

The class of functions (15) covers all stable modulations $g(t)$ that are higher harmonics of the Bloch frequency (i.e., with frequency $\omega = lF$, $l \in \mathbb{N}$). Let us generalize the cyclic-time argument to Bloch-commensurate interactions $g(t)$ evolving at a frequency $\omega = lF/\nu$ (i.e., with period $\nu T_B/l$), where $\nu, l \in \mathbb{N}$ are coprime. The common period with $\cos(Ft)$ is then $T = \nu T_B$.

We seek to factorize both the oscillating mass and interaction in the form

$$\cos(Ft) = \dot{\eta} M(\eta), \quad (18)$$

$$g(t) = \dot{\eta} P(\eta), \quad (19)$$

in terms of a suitable cyclic time $\eta(t)$ and otherwise arbitrary functions M and P . Then, the $\dot{\eta}$ drops out of Eq. (10), which can be written in terms of the cyclic time η only:

$$i \partial_\eta \tilde{A} = -M(\eta) \partial_z^2 \tilde{A} + P(\eta) |\tilde{A}|^2 \tilde{A}. \quad (20)$$

Its solution may be slightly more complicated than that of Eq. (16) but, again, $A(z, t) = \tilde{A}(z, \eta(t))$ is periodic because of the periodicity of $\eta(t)$.

In order to achieve the factorization (18) and (19), we observe that trigonometric identities permit writing $\cos Ft = \pm \sin \nu \tau = \pm \sin \tau M_\nu(\cos \tau)$, with a polynomial M_ν of degree $\nu - 1$, in terms of one of the slower angles τ defined via $\nu \tau = Ft \pm \pi/2 \pmod{2\pi}$ or, equivalently,

$$\tau = \tau_{\nu j}(t) = \frac{1}{\nu} \left[Ft - \frac{\pi}{2} (2j + 1) \right], \quad j \in \mathbb{Z}. \quad (21)$$

Defining $\eta = \cos \tau$ and $M(\eta) = (-1)^j (\nu/F) M_\nu(\eta)$ then gives Eq. (18). And from Eq. (19), we conclude that all modulations of the form

$$g(t) = \sin \tau \tilde{P}(\cos \tau), \quad (22)$$

with arbitrary $\tilde{P}(\eta) = -(F/\nu)P(\eta)$, guarantee stable modulated Bloch oscillations. This is equivalent to two conditions [24]:

(1) $g(t)$ has two common zeros with $\cos(Ft)$; namely $t = t_0, t_0 + T/2$, which are the zeros of $\sin \tau$ [see Eq. (21)].

(2) $g(t)$ is odd with respect to these points, $g(t_0 + t') = -g(t_0 - t')$, and similar for $t_0 + T/2$.

Let us illustrate how to construct such a stable modulation via the example of a $g(t)$ that is harmonically modulated with frequency ratio $\omega/F = l/\nu = 2/3$, as shown in Fig. 2. The commensurability $\nu = 3$ and the choice $j = 1$ determine $\tau = \tau_{31}(t) = (Ft - 3\pi/2)/3$, and from there the cyclic time $\eta = \cos \tau$. According to Eq. (22), a harmonic modulation with the desired frequency ratio is $g(t) = g_0 \sin 2\tau = 2g_0 \sin \tau \cos \tau$. Then, the wave function A is a function of η only, as shown in the right panel of Fig. 2.

Similarly, any harmonic modulation that is commensurate with the Bloch frequency, $\cos[(l/\nu)Ft + \delta]$, can be constructed. If the interaction is

$$g(t) = g_0 \sin(l \tau_{\nu j}(t)) = g_0 \sin \left\{ \frac{l}{\nu} \left[Ft - \frac{\pi}{2} (2j + 1) \right] \right\}, \quad (23)$$

with $\nu, l, j \in \mathbb{N}$, then the BO is stable. In Ref. [24], this result has been derived in a different but equivalent way. The class of functions (23) covers all frequencies commensurate with the Bloch frequency, if only the phase with respect to the BO is adjusted correctly (see Sec. VB and Fig. 5 below).

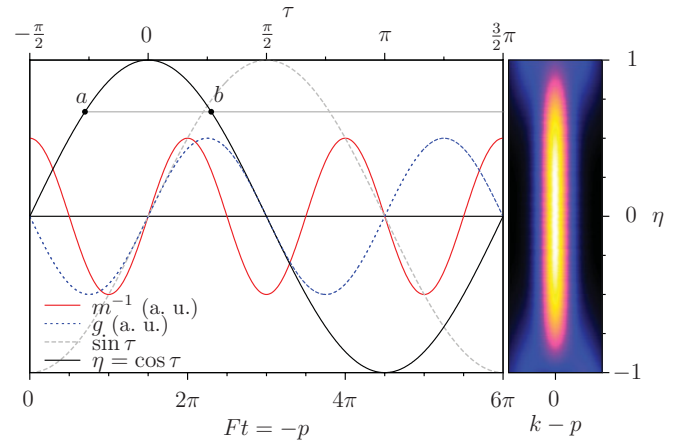


FIG. 2. (Color online) Time evolution scheme for a stable modulation $g(t)$ with frequency ratio $l/\nu = 2/3$. The common nodes of $m(t)^{-1} = 2 \cos(Ft)$ and $g(t)$ are shared by $\sin \tau$, with $\tau = \tau_{31}(t) = (Ft - 3\pi/2)/3$ [cf. Eq. (21)]. As required by Eq. (22), the interaction can be written as $g(t) = 2g_0 \sin \tau \cos \tau = g_0 \sin[2F(t - 3T_B/4)/3]$. Thus, the envelope function is a function of $\eta = \cos \tau$ only and is consequently periodic in t . The right panel shows the momentum space density $|\Psi_k|^2$, obtained by numerical integration of Eq. (5) with initial condition (6) and $\sigma_0 = 10$. The points in time with the same value of η , like a and b , show the same distribution. Parameters are $g_0 = 5$, $F = 0.2$.

D. Beyond the smooth-envelope approximation

The cyclic-time argument discussed above is based on the NLSE (10), where higher-than-second-order spatial derivatives have been neglected. We still need to estimate the effects caused by the third-order derivative.

In the *linear case*, each Fourier component can be treated separately, just as in Sec. III A. The third derivative shows up in

$$\begin{aligned} i\partial_t A_k &= k^2 \left(\cos Ft + \frac{k \sin Ft}{3} \right) A_k \\ &= k^2 \sqrt{1 + k^2/9} \cos(Ft - \phi_k) A_k, \end{aligned} \quad (24)$$

with $\tan \phi_k = k/3$, which can be easily solved in terms of its own cyclic time $\eta_k(t) = \sin(Ft - \phi_k)$. The result is, of course, periodic,

$$A_k^{(0)}(t) = A_k(0)e^{-i\varphi_k(t)}, \quad (25)$$

where

$$\varphi_k(t) = \frac{1}{F} \left[k^2 \sin Ft + \frac{k^3}{3} (1 - \cos Ft) \right]. \quad (26)$$

The initial Gaussian wave packet (6) with $A_k(0) = \sqrt{2/\pi} \sqrt{\sigma_0} \exp(-k^2 \sigma_0^2)$ restricts the relevant values of k to be of the order σ_0^{-1} . Thus, corrections due to the third derivative are small for wide wave packets. The superposition of all $A_k(t)$ leads to a reduction of the bare real-space Bloch amplitude (9) by $\langle z \rangle \approx -[\cos(Ft) - 1]/(F\sigma_0^2)$, which is indeed the leading order of the full result given in Ref. [37].

Interaction $g(t) = g_0 \cos(Ft)$. What happens if interactions, as in Sec. III B, are included into Eq. (24)? The interaction term $g(t) \int dk' dq A_{k-q} A_{q-k'}^* A_{k'}/(2\pi)$ mixes all components, which consequently cannot be solved separately. On the other hand, the global cyclic-time argument from Sec. III B is also broken by the factor $(k/3) \sin(Ft)$ from the third derivative. Thus, we expect a decay of the BO, even if the interaction satisfies the cyclic-time criterion (15). This decay should scale as the product of g and some wide-wave-packet parameter related to σ_0^{-1} .

We estimate this decay analytically by considering the first-order correction $A_k^{(1)}(t) = a_k(t) \exp[-i\varphi_k(t)]$ to Eq. (25), due to $g(t) = g_0 \cos(Ft)$. To this end we integrate the equation of motion

$$\dot{a}_k = -i e^{i\varphi_k(t)} g_0 \cos(Ft) \int \frac{dk' dq}{2\pi} A_{k-q}^{(0)} (A_{q-k'}^{(0)})^* A_{k'}^{(0)}. \quad (27)$$

We take advantage of the wide wave packet and expand systematically in the parameter $\sigma_0^{-1} \sim k$. The interaction integral evaluates to $(2\pi)^{-1/4} (3\pi\sigma_0)^{-1/2} e^{-k^2 \sigma_0^2/3}$ plus terms of second order in k and σ_0^{-1} . The time integral of $e^{i\varphi_k(t)} \cos(Ft)$ over the Bloch period is nonzero only due to the phase shift $\phi_k \approx k/3$ between $\varphi_k(t)$ and $\cos(Ft)$. It is expressed in terms of the Bessel function of the first kind $J_1(k^2/F) \approx k^2/(2F)$. Finally, we get

$$a_k(T_B) = \left(\frac{\pi}{2} \right)^{\frac{1}{4}} \frac{-g_0 k^3}{3\sqrt{3}\sigma_0 F^2} \exp\left(-\frac{k^2 \sigma_0^2}{3} \right). \quad (28)$$

The relevant values of k are cut off by the exponential and scale as $k \propto \sigma_0^{-1}$. No matter what the sign of g_0 , the net growth of

the first-order correction (28) after one Bloch period deforms the wave packet and destroys the periodic dynamics of the BO. This leaves us with the general scaling of the lifetime

$$\frac{1}{T_{\text{life}}} \sim \frac{|a_k(T_B)|}{T_B} \propto \frac{|g_0|}{F\sigma_0^{3.5}}, \quad (29)$$

assuring very long lifetimes for sufficiently wide wave packets.

This result proves to be quite reliable, as we have checked by means of a direct integration of the tight-binding equation of motion (5) for several sets of parameters. Numerically, we defined the lifetime as the time when the momentum variance has doubled with respect to its initial value. This includes averaging over the contributions of many modes and dynamics that go already quite far away from the original perturbative perspective. Still, we find this lifetime to scale as predicted by Eq. (29), with proportionality factor ≈ 0.2 .

IV. COLLECTIVE COORDINATES

From Sec. III, we know which modulations $g(t)$ should lead to stable BOs. But we wish to gain more quantitative information on how position and momentum distributions depend on the modulation. Moreover, we would like to describe the time evolution also in the unstable cases. Toward this aim, we employ the CC approach, as introduced in Ref. [26].

A. Equations of motion

The equation of motion (5) is derived as $i\Psi_n = \partial H/\partial \Psi_n^*$ from the mean-field Hamiltonian

$$H = \sum_n \left[-(\Psi_{n+1} \Psi_n^* + \text{c.c.}) + Fn |\Psi_n|^2 + \frac{g(t)}{2} |\Psi_n|^4 \right], \quad (30)$$

where Ψ_n and $i\Psi_n^*$ are canonically conjugate variables. Instead of describing all these amplitudes, we restrict the number of degrees of freedom and parametrize the dynamics of a smooth wave packet by its centroid $x(t) = \langle n \rangle = \sum_n n |\Psi_n(t)|^2$ and variance $w(t) = \langle [n - x(t)]^2 \rangle$. One also needs their respective conjugate momenta $p(t)$ and $b(t)$, defined by their generating role $-i\partial_p \Psi_n = n \Psi_n$ and similarly for b . Thus, we employ the ansatz

$$\Psi_n(t) = \frac{1}{\sqrt{w}} \mathcal{A} \left(\frac{n-x}{\sqrt{w}} \right) e^{ipn + ib(n-x)^2}, \quad (31)$$

with an even envelope function $\mathcal{A}(u)$ that is normalized according to $\int du |\mathcal{A}(u)|^2 = 1$ and $\int du u^2 |\mathcal{A}(u)|^2 = 1$. The assumptions underlying the CC description (31) differ slightly from the smooth-envelope ansatz [Eq. (7)]. Keeping a fixed wave-packet shape $\mathcal{A}(u)$ is of course more restrictive. On the other hand, the centroid x is now a free dynamical variable, which gives enhanced flexibility compared with the purely kinematic $x(t)$ of Eq. (9).

Inserting the CC ansatz (31) into the Hamiltonian (30), Taylor-expanding the discrete gradient to second order, and performing the sum as a continuous integral, one finds the effective Hamiltonian

$$H_{\text{cc}} = Fx - 2 \cos p \left(1 - \frac{K + 4b^2 w^2}{2w} \right) + I \frac{g(t)}{\sqrt{w}}, \quad (32)$$

TABLE I. Collective-coordinate parameters for Gaussian and soliton wave packets.

	$\mathcal{A}(u)$	K	I
Gaussian	$(2\pi)^{-1/4} e^{-u^2/4}$	$\frac{1}{4}$	$\frac{1}{4\sqrt{\pi}}$
Soliton	$\sqrt{\frac{\pi}{4\sqrt{3}}} [\cosh(\frac{\pi u}{2\sqrt{3}})]^{-1}$	$\frac{1}{4}(\frac{\pi}{3})^2$	$\frac{1}{4\sqrt{\pi}}(\frac{\pi}{3})^{3/2}$

with the kinetic integral $K = \int du |\mathcal{A}'(u)|^2$ and the interaction integral $I = (1/2) \int du |\mathcal{A}(u)|^4$. In Table I, these are given for a Gaussian and for a soliton-shaped wave packet.

By construction, the CC variables obey the canonical equations of motion

$$\dot{p} = -\frac{\partial H_{cc}}{\partial x} = -F, \quad (33)$$

$$\dot{x} = \frac{\partial H_{cc}}{\partial p} = 2 \sin p \left[1 - \frac{K + 4b^2 w^2}{2w} \right], \quad (34)$$

$$\dot{b} = -\frac{\partial H_{cc}}{\partial w} = \frac{K - 4w^2 b^2}{w^2} \cos p + \frac{I g(t)}{2w^{3/2}}, \quad (35)$$

$$\dot{w} = \frac{\partial H_{cc}}{\partial b} = 8wb \cos p. \quad (36)$$

In our study, the following initial conditions are considered: $x(0) = 0$, $p(0) = 0$, $w(0) = \sigma_0^2$, and $b(0) = 0$. Equation (33) shows that the driving term in all the equations is $p(t) = -Ft$, as already used in Eq. (8), and this independently of the interaction. In other words, the Bloch period is not affected by the atom-atom interaction. Furthermore, the dynamics of $b(t)$ and $w(t)$ is completely defined by the autonomous Eqs. (35) and (36), whose solution then determines the centroid motion according to Eq. (34).

In cold-atom experiments, time-of-flight images provide the momentum distribution of the atomic cloud. Therefore, it is appropriate to study not only the average (quasi) momentum p , but also the momentum variance, whose growth in time serves as a good indicator for the decay of the wave packet. Actually, the momentum variance already appears naturally in the effective Hamiltonian (32). Indeed, the kinetic energy contribution is nothing but the mean-field expectation $-\langle e^{i\hat{p}} + e^{-i\hat{p}} \rangle$ of (minus twice the real part of) the discrete translation operator. For a sufficiently narrow momentum distribution, this contributes

$$\langle \cos \hat{p} \rangle \approx \cos p \left(1 - \frac{(\Delta p)^2}{2} \right). \quad (37)$$

Comparing with the second term on the right-hand side of Eq. (32), we recognize $(\Delta p)^2 = K/w + 4b^2 w$. In passing, we note that this implies that $K = (\Delta x)^2 (\Delta p)^2 - 4b^2 (\Delta x)^4$ is a constant of motion. Since the wave packet has a fixed shape, this quantity can only be the surface of the uncertainty ellipse, $K = (\Delta x)^2 (\Delta p)^2 - (\Delta x p)^2$, so that we can identify $4b^2 = (\Delta x p)^2 / (\Delta x)^4$.

In terms of the momentum variance $r := (\Delta p)^2$, the equation of motion (34) for the centroid looks slightly simpler:

$$\dot{x} = -2 \left(1 - \frac{r}{2} \right) \sin(Ft). \quad (38)$$

The momentum variance obeys the equation of motion

$$\dot{r} = 4I g(t) b w^{-1/2}. \quad (39)$$

In the linear case $g = 0$, the momentum variance is a constant of motion, $(\Delta p)^2 = r_0 = K/\sigma_0^2$.¹ In this case, Eq. (38) integrates to $x(t) = (2/F)(1 - r_0/2)[\cos(Ft) - 1]$. Compared to the lowest-order result [Eq. (9)], the amplitude of the BO is found to be reduced by the finite momentum width, in agreement with the exact solution for Gaussian wave packets of arbitrary width, where the amplitude is reduced by a factor $e^{-r_0/2}$ [37]. Furthermore, Eqs. (35) and (36) yield the exact solution $w(t) = \sigma_0^2 + 4K \sin^2(Ft)/(F\sigma_0^2)$, which agrees with Eq. (14).

B. Interaction effects

Let us now study the CC equations (33)–(36) in the interacting case for several different modulations of the interaction parameter $g(t)$. In all of the following examples, we compare the CC results to the full integration of the tight-binding equation. Furthermore, we analytically isolate the leading-order effects caused by the interaction. We take advantage of the wide-wave-packet condition, $F\sigma_0^2 \gg 1$, and treat the interaction g perturbatively. To zeroth order in g and $1/(F\sigma_0^2)$, we have $w(t) = \sigma_0^2$ and $b(t) = 0$. Then, we compute the leading corrections via Eq. (35) and subsequently Eqs. (38) and (39), or Eq. (36).

1. Constant interaction

Constant interaction $g(t) = g_0$ is known to cause momentum broadening and damping [26,34]. From Eq. (35), we find the averaged linear increase $\overline{\dot{b}(t)} = I g_0 t / (2\sigma_0^3)$. Here and in the following, the overline denotes coarse graining over one Bloch period. Via Eqs. (39) and (38), we find

$$\overline{r(t)} \approx r_0 + \frac{I^2 g_0^2 t^2}{\sigma_0^4}, \quad (40)$$

$$x(t) \approx \frac{2}{F} \left\{ \left[1 - \frac{\overline{r(t)}}{2} \right] \cos(Ft) - \left[1 - \frac{r_0}{2} \right] \right\}, \quad (41)$$

which is consistent with Refs. [26,34]. In Fig. 3, we compare this perturbative result to the full CC prediction (33)–(36) and to the results from the integration of the discrete Gross-Pitaevskii equation (5). The approximation (41) initially agrees nicely with the CC prediction (33)–(36). The zoomed envelope of the centroid motion, shown in the inset, reveals, however, that the CC approach initially ($t \lesssim 15T_B$) underestimates the damping with respect to the full result. This is because the CC ansatz misses momentum broadening and energy losses due to degrees of freedom not included in the ansatz. At later times $t \gtrsim 20T_B$, the CC approach overestimates the damping. At this

¹The entire momentum distribution remains unchanged, up to the uniform translation $p = -Ft$, across the Brillouin zone, as can be seen from the reasoning in Sec. III D: even if arbitrarily high derivatives are included in the first line of Eq. (24), the Fourier components A_k do not mix; each of them acquires only a phase factor and $|\Psi_{k-p}|^2 = |A_k|^2$ is stationary.

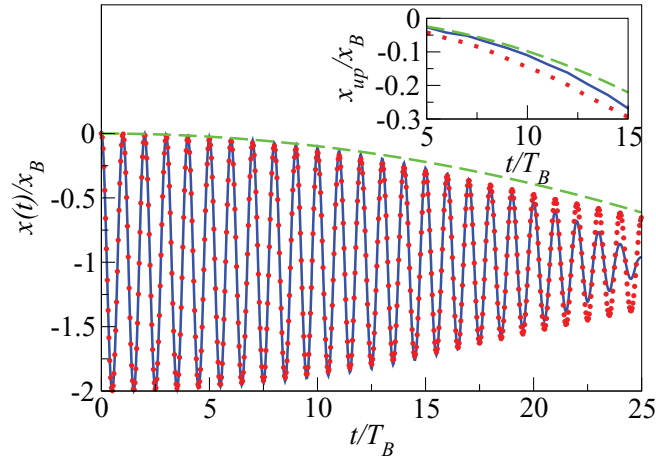


FIG. 3. (Color online) Centroid motion of a Gaussian wave packet for constant interaction $g(t) = g_0$, obtained by numerical integration of the full tight-binding equation of motion (5) (red dots) and CC approach (33)–(36) (solid blue). The dashed (green) line shows the upper turning points of the centroid within the perturbative result (41), $x_{\text{up}} = -(\bar{r} - r_0)/F$. The inset shows these upper turning points on a larger scale. Parameters are $F = 0.2$, $g_0 = 1.0$, and $\sigma_0 = 10$.

time, the CC ansatz already begins to break down, because the wave packet loses its shape [Fig. 1(b)].

2. Harmonic modulation

Let us now use the CC ansatz to understand the examples of the harmonic modulations of the interaction parameter presented in Fig. 1.

(a) *Cosine modulation.* $g(t) = g_0 \cos(Ft)$ [Fig. 1(a)]: BOs are stable, in agreement with the cyclic-time argument of Sec. III. The breathing of the linear BO is due to the first term in Eq. (35). The cosine modulation of $g(t)$ in the second term enhances or suppresses this breathing. Indeed, the breathing amplitude in Eq. (14) gets multiplied by a factor $[1 + I\sigma_0 g_0/(2K)]$, which in our example of Fig. 1(a) evaluates to 2.82. Thus, the breathing induced by g_0 is considerably stronger than the linear breathing. Nevertheless, both the integration of the CC equations of motion and the analytical result are in perfect agreement with the full tight-binding equation, as shown in the upper panel of Fig. 4. Thus, in this case, where the shape of the wave packet is preserved, the CC approach proves to be a very powerful tool.

(b) *Sine modulation.* $g(t) = g_0 \sin(Ft)$ [Fig. 1(b)]: In the long run, the wave packet loses its shape, which cannot be accurately described by CCs. During the first few Bloch periods, however, the wave packet is still intact and we may use CCs to describe, for example, the width of the wave packet. The interaction $g(t)$ enters via Eq. (35) and induces $b(t) \approx K \sin(Ft)/(F\sigma_0^4) - I g_0 \cos(Ft)/(2F\sigma_0^3)$. Only the second term, proportional to g_0 , has a nonvanishing time average after multiplying by $\cos p = \cos(Ft)$ in the equation of motion (36), which leads to

$$\overline{w(t)} \approx \sigma_0^2 - 2 \frac{I g_0}{F \sigma_0} t. \quad (42)$$

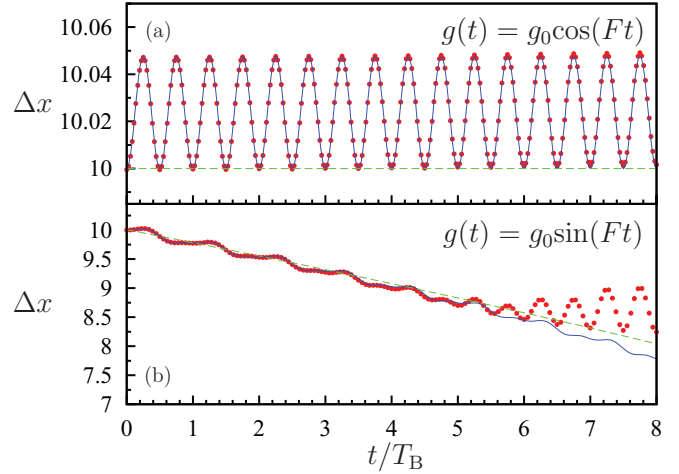


FIG. 4. (Color online) Width of the Bloch-oscillating wave packets of Fig. 1 ($F = 0.2$, $\sigma_0 = 10$, $g_0 = 1$). The respective curves show: Δx obtained from the tight-binding equation of motion (3) (red dots), the CC result $\Delta x = \sqrt{w}$ (solid blue), and the estimate $\sqrt{\bar{w}}$ from Eq. (42) (dashed green).

This prediction is shown in the lower panel of Fig. 4, together with the full solution of Eqs. (35) and (36) and the width extracted from the integration of the tight-binding equation of motion (5) [shown in Fig. 1(b)]. The CC description fares very well up to $t \approx 5T_B$. At this time the smooth shape of the wave packet is lost, and deviations from the CC prediction occur without surprise.

The change of the real-space variance (42) directly reflects in the change of the momentum variance, $r - r_0 = (\partial_w r) \Delta w \approx 2KI g_0 t/(F\sigma_0^5)$, driving the decay of the BO. Note that, for a modulation $g(t) \propto -\sin Ft$, the momentum variance initially decreases. Over the long run, however, the BO still decays, because the wave packet, does not maintain its shape, just as in the case of $+\sin Ft$.

C. Range of validity

In the above examples, we demonstrated that, under some limitations, the CC approach is capable of describing the principal degrees of freedom, position, and variance of a Bloch-oscillating wave packet. Since the CC ansatz relies on the shape $\mathcal{A}(u)$ of the wave packet [Eq. (31)] to be conserved, only the stable situations can be well described over the long run [see Fig. 4(a)]. In the unstable cases, CCs can describe only the initial dynamics, like the contraction of the wave packet shown in Fig. 4(b), but not the decay of its shape. For that task, we will pursue a different strategy in the following section.

V. LINEAR STABILITY ANALYSIS

We have already seen [Figs. 1(b) and 4(b)] that, in some cases, perturbations on a length scale much shorter than the width of the wave packet occur which ultimately destroy the BOs. The periodically time-dependent mass and interaction, as appearing in Eq. (10), provide the source of energy for the growth of such perturbations—a phenomenon known as *dynamical instability* [41,42]. In the following, we will employ Floquet theory to detect and to quantify the dynamical instability.

A. Lyapunov exponents for excitations

In order to quantitatively describe the growth of short-scale perturbations, we assume that the homogeneous background $\Psi_n^{(0)} = \sqrt{n_0}$ is dressed by small fluctuations $\delta\Phi_n \in \mathbb{C}$. We insert

$$\Psi_n = [\sqrt{n_0} + \delta\Phi_n] e^{ip(t)n} e^{-i\varphi(t)} \quad (43)$$

into Eq. (5) and expand in powers of $\delta\Phi_n$. To zeroth order, $p(t) = -Ft$ and $\dot{\varphi} = -2 \cos Ft + n_0 g(t)$. This solution describes an oscillating superfluid flow in a spatially homogeneous condensate (i.e., a δ peak in momentum space that performs perfect BOs), and this no matter how strong the interaction or how it is modulated. BOs only get dephased by a combination of inhomogeneity and interaction, as we find by looking at the first-order equation of motion for $\delta\Phi_n$. Similarly to the procedure leading to Eq. (10), we describe $\delta\Phi_{x(t)+z}$ in a moving reference frame $x(t) = (2/F)[\cos(Ft) - 1]$. This eliminates the first derivative of the Taylor expansion of $\delta\Psi_{n\pm 1}$. Third and higher derivatives are assumed to be small and are neglected. In the present approximation of a homogeneous background, the equations of motion for different Fourier components of the fluctuation decouple, and their real and imaginary parts $\Phi_k = s_k + id_k$ then have the coupled equations of motion

$$\dot{s}_k = k^2 \cos(Ft) d_k, \quad (44)$$

$$\dot{d}_k = -[k^2 \cos(Ft) + 2n_0 g(t)] s_k. \quad (45)$$

All these components contribute to the momentum variance

$$(\Delta p)^2 = \frac{1}{Nn_0} \sum_k k^2 (|s_k|^2 + |d_k|^2), \quad (46)$$

where N is the system size entering the discrete Fourier transformation. In unstable cases, some fluctuation with a certain k vector will possess the largest growth rate and therefore dominate the decay of BOs. In the following, we seek to determine the most unstable mode and its growth rate (i.e., Lyapunov exponent).

In the quasistatic picture, where the mass $\cos Ft = 1/(2m_0)$ and interaction g_0 are considered constant, the system of coupled equations (44) and (45) can be solved by a Bogoliubov transformation [43,44]: the elementary excitation

$$c_k = \sqrt{\omega_k/\omega_k^0} s_k + i\sqrt{\omega_k^0/\omega_k} d_k \quad (47)$$

defined in terms of single-particle dispersion $\omega_k^0 = k^2/(2m_0)$ and the Bogoliubov frequency

$$\omega_k = \sqrt{\omega_k^0(\omega_k^0 + 2g_0n_0)} \quad (48)$$

has the simple time evolution $c_k(t) \propto \exp(-i\omega_k t)$. The criterion for BO stability is then the following: If m_0 and g_0 are of the same sign, then ω_k is real for all k , and the extended condensate is stable. If, however, m_0 and g_0 have opposite signs, then imaginary frequencies occur for $k < k_* = 2\sqrt{n_0|g_0m_0|}$, indicating a modulational instability of the extended condensate. These modulations lead to the formation of bright solitons [39]. Consistent with this picture is that the critical wave number k_* , estimated from the central density $n_0 = 1/(2\xi)$, relates to the soliton width: $k_* = 2/\xi$.

But we have already seen in Sec. III B 2 that such a quasistatic stability criterion does not adequately describe the dynamical stability of Bloch oscillations with modulated interaction $g(t)$.

Let us then solve the time-dependent Eqs. (44) and (45) with harmonic $g(t)$. These are linear equations with time-periodic coefficients, which makes them accessible for Floquet theory [27], provided the frequency of the external modulation $g(t)$ is commensurate with the Bloch frequency $\omega_B = F$. Because the driving is periodic, integrating the equations of motion over a single period T yields all information necessary for the time evolution over $n \in \mathbb{N}$ periods:

$$\begin{pmatrix} s_k(t+nT) \\ d_k(t+nT) \end{pmatrix} = M_k^n \begin{pmatrix} s_k(t) \\ d_k(t) \end{pmatrix}. \quad (49)$$

The monodromy matrix

$$M_k = \begin{pmatrix} s_k^1(T) & s_k^2(T) \\ d_k^1(T) & d_k^2(T) \end{pmatrix} \quad (50)$$

contains the solution at time T starting from the two linearly independent initial conditions $\{s_k^1(0) = 1, d_k^1(0) = 0\}$ and $\{s_k^2(0) = 0, d_k^2(0) = 1\}$. From Eq. (49), it is clear that the eigenvalues ρ_k^\pm of M_k determine the growth of the perturbations. With the help of Liouville's formula $\det(M_k) = 1$, one finds

$$\rho_k^\pm = (\text{tr} M_k / 2) \pm \sqrt{(\text{tr} M_k / 2)^2 - 1}. \quad (51)$$

The Lyapunov exponent $\lambda_k = T^{-1} \ln[\max(|\rho_k^+|, |\rho_k^-|)]$ then characterizes the exponential growth of the amplitudes $s_k, d_k \sim e^{\lambda_k t}$. In the following, we explore the consequences of this description in some particularly relevant cases.

B. Robustness with respect to perturbations

1. Stability map

BOs are stable if the Lyapunov exponent λ_k vanishes for all k [24]. This is indeed the case if $g(t)$ fulfills Eq. (22), because the cyclic-time argument from Sec. III applies also in the present scope: All fluctuations s_k and d_k evolve periodically in time, and thus do not grow exponentially.

Specifically, a modulation $g(t) = g_0 \cos(\omega t + \delta)$ at any frequency ω commensurate with the Bloch frequency F allows for periodic BOs if the relative phase δ is adjusted properly [Eq. (23)]. In order to assess how precise this phase needs to be adjusted, we can study the growth of fluctuations with the help of Floquet theory by computing the lifetime $(\max_k \lambda_k)^{-1}$ for a certain, small phase shift of order 10^{-4} . For completeness, we also consider similarly small frequency detunings, although Floquet theory does not work because commensurability is broken, such that we need to integrate the system of equations (44) and (45) numerically. The lifetime is used as radius in the graphical representation in the δ - ω plane shown in Fig. 5. The stable points are arranged on a regular pattern, where the most robust points are arranged on lines. With increasing denominator ν , the robustness drops rapidly.

We observe a remarkable asymmetry of the robustness between $+\cos Ft$ and $-\cos Ft$. The stability of the $+\cos Ft$ modulation is much more robust than the stability of $-\cos Ft$. In the latter case, mass and interaction always have opposite sign and the quasistatic frequencies ω_k are imaginary for $k < k_*$. Thus, the perturbations grow and decay exponentially,

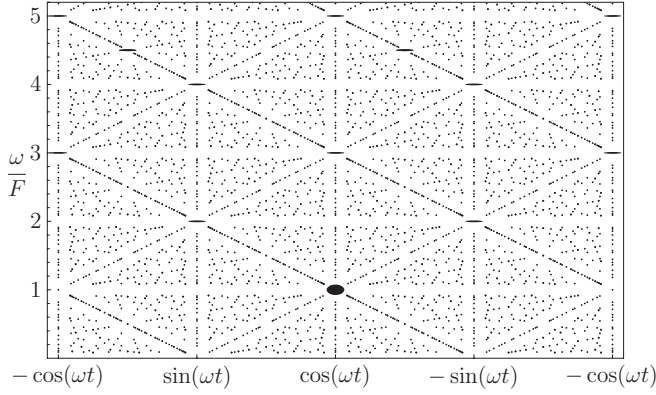


FIG. 5. BOs for commensurate harmonic modulation $g(t) = g_0 \cos(\omega t + \delta)$. The stable cases (δ_0, ω_0) , according to Eq. (23), are marked in the δ - ω plane. Frequencies $\omega = lF/v$ have been accounted for up to $v = 12$. The size of the ellipses represents the lifetime in the presence of a perturbation in phase ($\delta = \delta_0 + 10^{-4}$ rad) and in frequency [$\omega = \omega_0(1 + 10^{-4})$]. The largest radii correspond to a lifetime of $5T_B$ or more; the smallest to $1T_B$ or less. Parameters are $F = 0.2$ and $n_0 g_0 = 1$.

and their periodic return to the initial values relies solely on the cyclic-time argument. Due to this exponential growth, the case $-\cos Ft$ is much more susceptible to perturbations than is the case of $+\cos Ft$, which has only real frequencies. In the following, we will investigate this argument more quantitatively.

2. Perturbative Lyapunov exponents

We consider the Floquet problem (44) and (45) and search for analytical solutions at a given modulation $g(t) = g^{(0)}(t) + g^{(1)}(t)$. The component $g^{(0)}(t) = g_0 \cos Ft$ does not destabilize the periodic time evolution, while $g^{(1)}(t)$ is a perturbation term, which may contain several frequencies and phases. The unperturbed problem is conveniently solved using the cyclic time (11), which eliminates the time dependence $\cos Ft$. Then, the Bogoliubov transformation (47), with Eq. (48) and $2m_0 = 1$, yields the solution $c_k(\eta) \propto \exp(-i\omega_k \eta)$. It turns out to be handy to write the perturbed equation of motion for the excitation amplitude $\gamma_k = (c_k + c_{-k})/2$ with even parity (choosing the odd parity $-i(c_k - c_{-k})/2$ yields the same result as below):

$$i\dot{\gamma}_k = \cos(Ft)\omega_k \gamma_k + \frac{\omega_k^0}{\omega_k} n_0 g^{(1)}(t)(\gamma_k + \gamma_k^*). \quad (52)$$

So far, we have not made any approximation. Under the assumption that the perturbation only causes a weak growth of γ_k per period T , we now make the ansatz $\gamma_k(t) = [\gamma_k^0 + \gamma_k^1(t)] \exp[-i\omega_k \eta(t)]$ for the first-order correction $\gamma_k^1(t)$. In order to obtain the growth per total period T of the excitation γ_k , we need to determine

$$\frac{\gamma_k^1(T)}{\gamma_k^0} = \frac{n_0 \omega_k^0}{i\omega_k} \int_0^T dt g^{(1)}(t) \left(1 + \frac{\gamma_k^{0*}}{\gamma_k^0} e^{2i\omega_k \sin(Ft)/F} \right). \quad (53)$$

Within the present approximation of a homogeneous background, the constant in the brackets of Eq. (53) contributes only via the zero-frequency component of $g^{(1)}$, causing a mere

phase shift $\gamma_k^1 \propto i\gamma_k^0$, which may be dropped within the leading order.

We now expand the perturbation in its frequency components

$$g^{(1)}(t) = \sum_{v,l} \{g_{vl} \cos[l\tau_{v0}(t)] + \tilde{g}_{vl} \sin[l\tau_{v0}(t)]\}, \quad (54)$$

with $\tau_{v0}(t)$ from Eq. (21), and $v, l > 0$ and coprime. Within first-order perturbation theory, we may treat all contributions separately. In accordance with Eq. (23), the components \tilde{g}_{vl} have vanishing contribution to the growth of excitations. The cosine contributions, integrated according to Eq. (53) over a fundamental period $T = vT_B$, vanish for $v \neq 1$ and can be expressed in terms of Bessel functions J_l of the first kind for $v = 1$:

$$\frac{\gamma_k^1(T)}{\gamma_k^0} = \frac{\gamma_k^{0*}}{i\gamma_k^0} \frac{n_0 \omega_k^0}{\omega_k} \frac{2\pi}{F} \sum_l i^l g_{1l} J_l(2\omega_k/F). \quad (55)$$

The relative growth $|1 + \gamma_k^1(T)/\gamma_k^0|$ depends on the complex phase $\gamma_k^0/(\gamma_k^0)^* = e^{i\alpha}$. For the Lyapunov exponent, we are only interested in the fastest possible growth (i.e., we maximize with respect to α). From $e^{\lambda_k T} \approx 1 + \lambda_k T = 1 + \max_\alpha \text{Re}[\gamma_k^1(T)/\gamma_k^0]$ we then find

$$\lambda_k = \frac{n_0 \omega_k^0}{\omega_k} \left| \sum_l i^l g_{1l} J_l(2\omega_k/F) \right|. \quad (56)$$

Within the first order considered here, the growth of the excitations is caused only by the components $v = 1$ of Eq. (54) (i.e., integer multiples of the Bloch frequency). Other components $v > 1$ not fulfilling the cyclic-time condition (22) still cause perturbations to grow, but only as a second-order effect in the small parameter g . The different contributions in Eq. (56) may add up quite differently, depending on the amplitudes g_{1l} . Consequently, the most unstable modes may be located at different values of k .

3. Off-phase perturbation

The most prominent contribution to the Lyapunov exponent (56) is the Bloch periodic perturbation $\sin(Ft)$, as discussed in Ref. [25]. The Lyapunov exponent in the case of a Bloch periodic interaction $g(t) = g_0 \cos(Ft) + g_1 \sin(Ft)$ reads

$$\lambda_k = \left| g_1 n_0 \frac{\omega_k^0}{\omega_k} J_1 \left(\frac{2\omega_k}{F} \right) \right|, \quad (57)$$

with $\omega_k = [k^2(k^2 + 2g_0 n_0)]^{1/2}$ [Eq. (48) with $2m_0 = 1$]. Here, we can connect to the phase perturbation of the modulation $g(t) = \pm g_0 \cos Ft$, shown in the stability map of Fig. 5. We need to set $g_0 n_0 = \pm 1$ and $g_1 n_0 = 10^{-4}$. In the case $g_0 n_0 = +1$, the Bessel function in Eq. (57) oscillates rapidly as function of k , and the maximum Lyapunov exponent is found close to the sixth extremum of the Bessel function at $k \approx 1.03$ with the value $\lambda_*^+ \approx 0.00035 T_B^{-1}$. In the case $g_0 n_0 = -1$, ω_k becomes imaginary for $k < k_* = \sqrt{2}$, while the analytic continuation of ω_k^{-1} times the Bessel function remains real and regular. And indeed, the maximum Lyapunov exponent is found in the region of imaginary frequencies, at $k \approx 1.05$. There, the Lyapunov exponent $\lambda_*^- \approx 8.84 T_B^{-1}$ is much larger than λ_*^+ , which explains the asymmetry already observed

in Fig. 5. Put differently, we find that the $+\cos$ modulation enhances the robustness against the sine perturbation, whereas the $-\cos$ modulation reduces it.

4. Robustness against general noise

Let us come back to the more general noise (54) and the prediction for the perturbation growth (56). We address two questions: To what extent can the robustness be enhanced in this case? Do the predictions hold in realistic systems where the wave packet is wide but finite?

We thus confront the analytical result with a Gross-Pitaevskii integration [Eq. (5)], where the interaction $g(t)$ is composed of a noise term of type (54) plus a deliberate modulation $g(t) = g_0 \cos Ft$. We consider different values of g_0 , which in the clean case define

- (i) the linear BO, $g_0 = 0$;
- (ii) the breathing wave packet, $g_0 > 0$;
- (iii) the rigid soliton, $g_0 = g_r < 0$ [see Eq. (17)];
- (iv) the antibreathing wave packet, $g_0 < g_r$.

In Fig. 6, the momentum variance is shown, which signals the decay of the wave packet and destruction of BOs. In all cases, the momentum distribution starts to broaden at some time. Thereby, the breathing wave packet shows a much longer lifetime than the linear and the rigid case, whereas the antibreathing wave packet lives much shorter. As conjectured above, the $+\cos$ modulation indeed stabilizes the BOs against the noise of the interaction parameter $g(t)$.

In order to quantitatively verify the prediction (56), we examine the momentum density of the wave packets, as shown

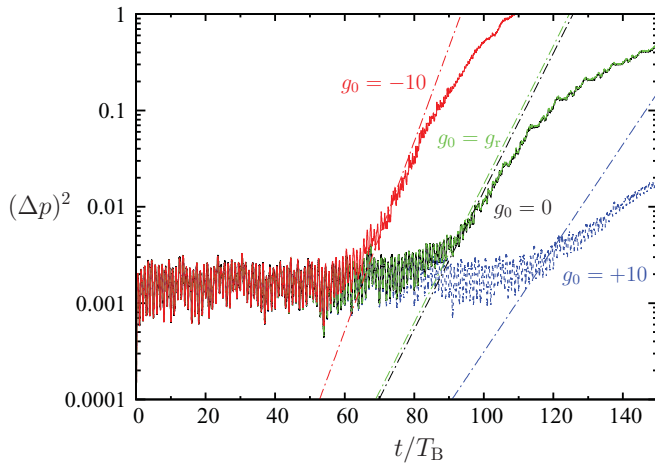


FIG. 6. (Color online) Momentum variance $(\Delta p)^2$ of a wave packet of soliton shape (17) with initial spatial width $\xi = 66.16$ (a small seed noise of 10^{-3} mimics experimental inhomogeneities), Bloch-oscillating in a tilted lattice with $F = 0.2$. The interaction parameter is modulated as $g(t) = g^{(1)}(t) + g_0 \cos(Ft)$ for a random perturbation $g^{(1)}(t)$ of type (54) with frequencies $\Omega_l = lF/\nu$ below and above the Bloch frequency, $\nu = 8$, $l = 1, 2, \dots, \nu^2$. The coefficients g_{vl} , and \tilde{g}_{vl} are random numbers with zero mean and standard deviation 0.4, except for $g_{\nu\nu} = 0.5$ and $\tilde{g}_{\nu\nu} = 0$ (overwritten by $-g_0$). The dash-dotted lines show the slope predicted by the Lyapunov exponent $\lambda = 2 \max_k \lambda_k$ [cf. Eq. (51)]. As g_0 is varied from -10 (antibreathing) over $g_r = -0.06$ (rigid) and 0 (linear) [nearly overlapping with g_r] to $+10$ (breathing), the predicted slope decreases and the observed lifetime increases.

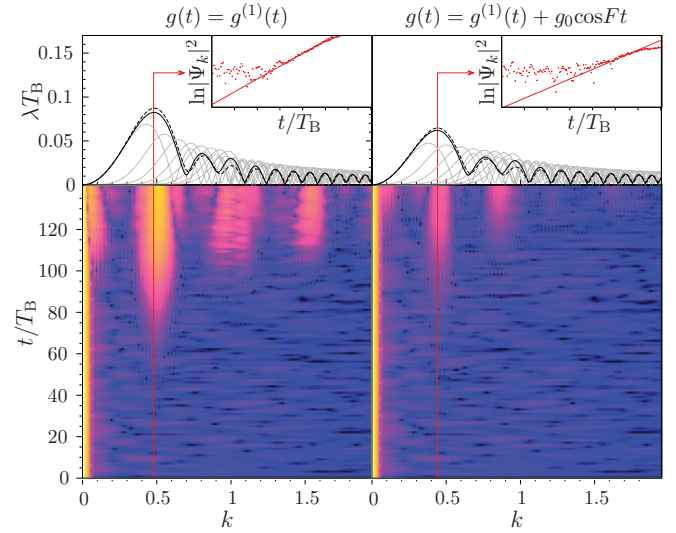


FIG. 7. (Color online) Momentum-space portrait of decaying BOs in presence of a particular realization of the random perturbation $g^{(1)}(t)$ of type (54), without (left) and with (right) an additional cosine-like modulation ($g_0 = 10$). (Upper panel) Lyapunov exponents from Eq. (51) (solid black), and the perturbative result (56) (dashed black), which is composed of the contributions from the individual frequency components $0.5n_0\omega_k^0 |J_l(2\omega_k/F)|/\omega_k$ (thin gray). (Lower panel) Stroboscopic plot of the k -space density on a logarithmic color scale [prediction from full Floquet theory (51)]. Parameters are the same as in Fig. 6. Clearly, the harmonic modulation stabilizes the BOs against residual fluctuations of the interaction parameter.

in Fig. 7 for the nonmodulated and the breathing wave packet. We can compare the growth obtained from Eq. (51) and the analytical prediction (56) to the growth obtained by integrating the full Gross-Pitaevskii equation (5). Indeed, the growth of the dominantly growing mode (marked with a vertical line in Fig. 7) agrees with the largest predicted Lyapunov exponents. Beyond that, the full momentum-space distribution shows the finite width of the central wave packet and higher harmonics of the dominant mode due to the nonlinearity of the Gross-Pitaevskii equation (5).

For momentum broadening (Fig. 6), the accurate description of the fastest-growing mode is sufficient. Thus, Eq. (56) gives a satisfactory description of the BO decay. In conclusion, we have confirmed our prediction from above that the $+\cos$ modulation of $g(t)$ significantly stabilizes the BO.

C. Range of validity

The linear stability analysis presented in this section is based on the infinitely extended wave packet, and thus can only be expected to work for rather wide wave packets, as in the example of Figs. 6 and 7. In other words, the *wide wave packet* assumption means that the excitations are well separated (in k space) from the main wave packet.

Interactions $g(t)$ with nonzero time average, like $g(t) = g_0$, act directly on the width degree of freedom, as discussed in Sec. IV B. In this case, the homogeneous stability analysis is not reliable, because the most important degree of freedom is missed. Indeed, the momentum width $\Delta p = \sqrt{r}$ increases

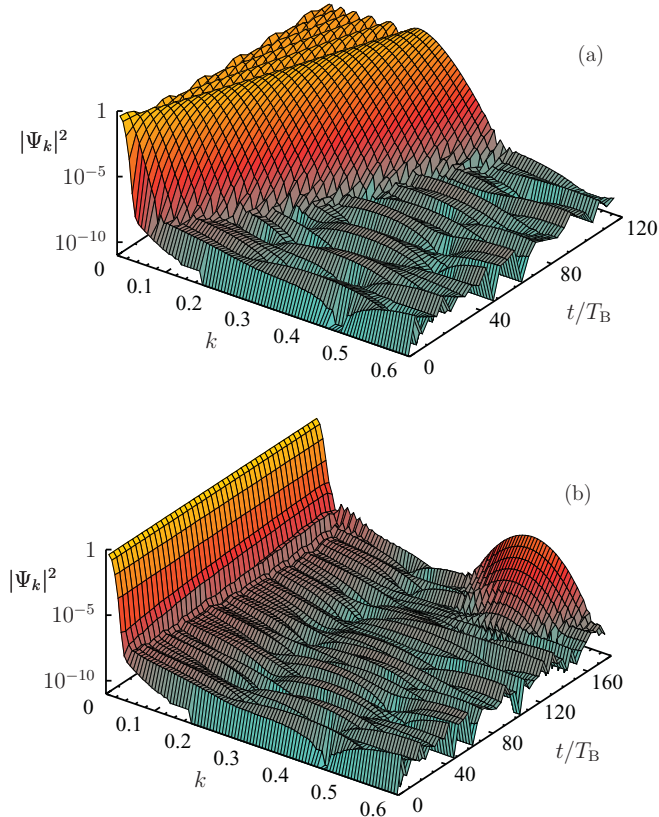


FIG. 8. (Color online) Stroboscopic plot of the momentum density $|\Psi_k|^2$ in unstable cases. (a) $g(t) = g_0$. The immediate broadening of the wave packet in k space is not compatible with the assumptions of our linear stability analysis, whose starting point is an infinitely extended wave function in real space. (b) $g(t) = g_0 \sin(Ft)$. The most unstable mode, which dominates the decay, is well separated from the central wave packet. In both cases, the original wave function is centered around $k = 0$ with width $\sigma_0 = 100$, $F = 0.2$, and $g_0 = 2.5$.

linearly with time, as pointed out in Sec. IV B [Eq. (40)]. Figure 8(a) shows exactly this: In the case of constant nonlinearity, the central wave packet is spreading from the start and soon covers a large range in momentum space such that one cannot consider excitations separated from the central wave packet. In this case, the dynamics is better described by the collective coordinates approach of Sec. IV. Both approaches must be considered complementary to each other to describe a wide range of situations.

On the contrary, Fig. 8(b) shows that, in the case of sine perturbation, the perturbations remain well separated from the central wave packet. In this case and in the other cases with vanishing mean of $g(t)$, the linear stability analysis proves to be very powerful.

VI. CONCLUSIONS

We have treated the problem of BOs with a time-dependent interaction in the mean-field framework of the one-dimensional tight-binding model. This description applies to a dilute Bose gas in a deep lattice potential with a strong transverse confinement, as well as to arrays of nonlinear optical waveguides. Interestingly, the stability of BOs in the presence

of modulated interactions is sensitively conditioned on the relative phase between modulation and BO.

Our analysis shows that the linear BO already has a breathing width, but its momentum-space distribution is time independent (up to the uniform translation $p = -Ft$). For sufficiently wide wave packets, a cyclic-time argument allows us to identify a class of interactions $g(t)$ that lead to periodic dynamics, in spite of the interaction. In these cases, both real-space and momentum-space distributions become time dependent, but return periodically to the initial state. In all other cases, the BO decays with simultaneous momentum-space broadening. The broadening is either due to the broadening of the central (k -space) wave packet or due to the growth of excitations separated from the central wave packet.

In order to quantitatively describe both the periodic cases and the decay, we have employed two complementary methods: the *collective-coordinates* approach and the *linear stability analysis* of the extended wave packet. The collective-coordinates approach is valid as long as the shape of the wave packet is essentially conserved. It is capable of describing, on the one hand, the centroid and the breathing dynamics in the periodic cases and, on the other hand, the beginning of the decay in the unstable cases; for example, at constant interaction. The linear stability analysis of the extended wave packet is suitable for the quantitative description of the decay of wide wave packets, when the relevant excitations are well decoupled in k space from the original wave packet. Together, the two approaches provide a rather complete picture of the wave-packet dynamics.

The most striking prediction due to the linear stability analysis is that a cosine modulation of the interaction (the one that enhances the breathing) makes the BO more robust with respect to certain perturbations. This works especially well for a fluctuating residual interaction with zero time average, as in Figs. 6 and 7. However, the modulation has little effect on the decay due to a finite offset of the interaction. The strategy for achieving long-living BOs is to tune the interaction to zero as well as possible and then employ the cosine modulation to minimize the effect of residual fluctuations around zero.

Conversely, we conjecture that the enhanced phase sensitivity of nonlinear BOs (similar to the effect of harmonically shaken lattices in the linear case [45]) may become useful to design high-precision matter-wave interferometers.

ACKNOWLEDGMENTS

This work was supported in Madrid by Ministerio de Ciencia e Innovación (MICINN) (projects MOSAICO and MAT2010-17180) and in Singapore by the National Research Foundation & Ministry of Education. C.G. acknowledges funding from CEI Campus Moncloa, PICATA program. R.P.A.L. acknowledges financial support from Conselho Nacional de Desenvolvimento Científico e Tecnológico (CNPq). C.G. and C.A.M. acknowledge financial support from Deutsche Forschungsgemeinschaft (DFG) for the time when both were affiliated with the Universität Bayreuth. Travel between Bayreuth and Madrid was supported by the joint program Acciones Integradas of Deutscher Akademischer Auslandsdienst (DAAD) and MICINN.

- [1] B. P. Anderson and M. A. Kasevich, *Science* **282**, 1686 (1998).
- [2] F. Cataliotti, S. Burger, C. Fort, P. Maddaloni, F. Minardi, A. Trombettoni, A. Smerzi, and M. Inguscio, *Science* **293**, 843 (2001).
- [3] O. Morsch, J. H. Müller, M. Cristiani, D. Ciampini, and E. Arimondo, *Phys. Rev. Lett.* **87**, 140402 (2001).
- [4] C. Zener, *Proc. R. Soc. London A* **145**, 523 (1934).
- [5] F. Bloch, *Z. Phys.* **52**, 555 (1929).
- [6] M. Ben Dahan, E. Peik, J. Reichel, Y. Castin, and C. Salomon, *Phys. Rev. Lett.* **76**, 4508 (1996).
- [7] S. R. Wilkinson, C. F. Bharucha, K. W. Madison, Q. Niu, and M. G. Raizen, *Phys. Rev. Lett.* **76**, 4512 (1996).
- [8] H. Lignier, C. Sias, D. Ciampini, Y. Singh, A. Zenesini, O. Morsch, and E. Arimondo, *Phys. Rev. Lett.* **99**, 220403 (2007).
- [9] A. Eckardt, C. Weiss, and M. Holthaus, *Phys. Rev. Lett.* **95**, 260404 (2005).
- [10] E. Haller, R. Hart, M. J. Mark, J. G. Danzl, L. Reichsöllner, and H.-C. Nägerl, *Phys. Rev. Lett.* **104**, 200403 (2010).
- [11] J. Feldmann, K. Leo, J. Shah, D. A. B. Miller, J. E. Cunningham, T. Meier, G. von Plessen, A. Schulze, P. Thomas, and S. Schmitt-Rink, *Phys. Rev. B* **46**, 7252 (1992).
- [12] K. Leo, P. H. Bolivar, F. Brüggemann, R. Schwedler, and K. Köhler, *Solid State Commun.* **84**, 943 (1992).
- [13] L. Khaykovich, F. Schreck, G. Ferrari, T. Bourdel, J. Cubizolles, L. D. Carr, Y. Castin, and C. Salomon, *Science* **296**, 1290 (2002).
- [14] E. Tiesinga, B. J. Verhaar, and H. T. C. Stoof, *Phys. Rev. A* **47**, 4114 (1993).
- [15] M. Gustavsson, E. Haller, M. J. Mark, J. G. Danzl, G. Rojas-Kopeinig, and H.-C. Nägerl, *Phys. Rev. Lett.* **100**, 080404 (2008).
- [16] E. Timmermans, P. Tommasini, M. Hussein, and A. Kerman, *Phys. Rep.* **315**, 199 (1999).
- [17] T. Köhler, K. Góral, and P. S. Julienne, *Rev. Mod. Phys.* **78**, 1311 (2006).
- [18] C. Chin, R. Grimm, P. Julienne, and E. Tiesinga, *Rev. Mod. Phys.* **82**, 1225 (2010).
- [19] S. E. Pollack, D. Dries, R. G. Hulet, K. M. F. Magalhães, E. A. L. Henn, E. R. F. Ramos, M. A. Caracanhas, and V. S. Bagnato, *Phys. Rev. A* **81**, 053627 (2010).
- [20] I. Vidanović, A. Balaž, H. Al-Jibbouri, and A. Pelster, *Phys. Rev. A* **84**, 013618 (2011).
- [21] R. Morandotti, U. Peschel, J. S. Aitchison, H. S. Eisenberg, and Y. Silberberg, *Phys. Rev. Lett.* **83**, 4756 (1999).
- [22] T. Pertsch, P. Dannberg, W. Elflein, A. Bräuer, and F. Lederer, *Phys. Rev. Lett.* **83**, 4752 (1999).
- [23] R. Sapienza, P. Costantino, D. Wiersma, M. Ghulinyan, C. J. Oton, and L. Pavesi, *Phys. Rev. Lett.* **91**, 263902 (2003).
- [24] C. Gaul, R. P. A. Lima, E. Díaz, C. A. Müller, and F. Domínguez-Adame, *Phys. Rev. Lett.* **102**, 255303 (2009).
- [25] E. Díaz, C. Gaul, R. P. A. Lima, F. Domínguez-Adame, and C. A. Müller, *Phys. Rev. A* **81**, 051607R (2010).
- [26] A. Trombettoni and A. Smerzi, *Phys. Rev. Lett.* **86**, 2353 (2001).
- [27] N. G. Markley, *Principles of Differential Equations* (Wiley, Hoboken, 2004).
- [28] F. Dalfovo, S. Giorgini, L. P. Pitaevskii, and S. Stringari, *Rev. Mod. Phys.* **71**, 463 (1999).
- [29] K.-P. Marzlin and V. I. Yukalov, *Eur. Phys. J. D* **33**, 253 (2005).
- [30] O. Morsch and M. Oberthaler, *Rev. Mod. Phys.* **78**, 179 (2006).
- [31] A. Smerzi and A. Trombettoni, *Phys. Rev. A* **68**, 023613 (2003).
- [32] B. Mendez and F. Domínguez-Adame, *J. of Phys. A* **24**, L331 (1991).
- [33] Q. Niu, X.-G. Zhao, G. A. Georgakis, and M. G. Raizen, *Phys. Rev. Lett.* **76**, 4504 (1996).
- [34] D. Witthaut, M. Werder, S. Mossmann, and H. J. Korsch, *Phys. Rev. E* **71**, 036625 (2005).
- [35] G. P. Agrawal, *Nonlinear Fiber Optics* (Academic Press, Boston, 2007).
- [36] M. Salerno, V. V. Konotop, and Y. V. Bludov, *Phys. Rev. Lett.* **101**, 030405 (2008).
- [37] T. Hartmann, F. Keck, H. J. Korsch, and S. Mossmann, *New J. Phys.* **6**, 2 (2004).
- [38] F. Domínguez-Adame, *Eur. J. Phys.* **31**, 639 (2010).
- [39] V. V. Konotop and M. Salerno, *Phys. Rev. A* **65**, 021602 (2002).
- [40] Y. V. Bludov, V. V. Konotop, and M. Salerno, *J. Phys. B* **42**, 105302 (2009).
- [41] L. Fallani, L. De Sarlo, J. E. Lye, M. Modugno, R. Saers, C. Fort, and M. Inguscio, *Phys. Rev. Lett.* **93**, 140406 (2004).
- [42] B. Wu and Q. Niu, *New J. Phys.* **5**, 104 (2003).
- [43] C. Gaul and C. A. Müller, *Europhys. Lett.* **83**, 10006 (2008).
- [44] S. Giorgini, L. Pitaevskii, and S. Stringari, *Phys. Rev. B* **49**, 12938 (1994).
- [45] C. E. Creffield and F. Sols, *Phys. Rev. A* **84**, 023630 (2011).